Talanta 125 (2014) 393–399

Contents lists available at ScienceDirect

Talanta

journal homepage: www.elsevier.com/locate/talanta

Quantitative single-molecule detection of protein based on DNA tetrahedron fluorescent nanolabels

Yongshun Ding [a], Xingti Liu [a], Jing Zhu [a], Lei Wang [b], Wei Jiang [a,*]

[a] Key Laboratory for Colloid and Interface Chemistry of Education Ministry, School of Chemistry and Chemical Engineering, Shandong University, Jinan, 250100, PR China

[b] School of Pharmacy, Shandong University, Jinan, 250012, PR China

ARTICLE INFO

Article history:
Received 27 December 2013
Received in revised form
10 March 2014
Accepted 13 March 2014
Available online 24 March 2014

Keywords:
Single-molecule detection
Fluorescence imaging
DNA tetrahedron
Fluorescent nanolabel

ABSTRACT

A highly sensitive method for single-molecule quantitative detection of human IgG is presented by the employment of a new fluorescent nanolabel. In this method, fluorescent nanolabels were assembled by inserting SYBR Green I into DNA tetrahedron nanostructure. The bio-nanolabels were attached to the streptavidin-antihuman antibody by a specific reaction between biotin and streptavidin. The antibody was combined with the target antigen, human IgG, which was immobilized on the silanized glass subtrate surface. Finally, epi-fluorescence microscopy (EFM) coupled with an electron multiplying charge-coupled device was employed for fluorescence imaging. The fluorescent spots corresponding to single protein molecule on images were counted and further used for the quantitative detection. It was found that the new nanolabel shows good photostability, biocompatiblity and exhibits no blinking compared to traditional labels like fluorescence dyes and quantum dot (QDs). In addition, the number of fluorescence spots on the images has a linear relationship with the concentration of human IgG in the range of 3.0×10^{-14} to 1.0×10^{-12} mol L^{-1}. What is more, this method showed an excellent specificity and a low matrix effect.

1. Introduction

Single-molecule detection (SMD), based on the analysis of individual molecules, has attracted a great deal of attention in the fields of chemical analysis, biomedical research, and clinical diagnostics because SMD can provide a resolution that cannot be obtained with ensemble measurements in analytical chemistry [1–3]. In SMD, fluorescence imaging techniques, such as confocal fluorescence microscopy [4–7], total internal reflection fluorescence microscopy (TIRFM)[8–11] and epi-fluorescence microscopy (EFM) [12,13] are the most attractive methods due to sensitivity and immediateness [14]. In these fluorescence-based SMD studies, the quantification of targets relies on counting the single molecules rather than measuring the signal intensity [15]. On the assumption of target molecules being identified, the most important advantage of counting the single molecules is that the detected signal intensity is not very important, which guarantees the reliability of detection [16,17]. To ensure that the target molecules can be identified with exquisite sensitivity, suitable fluorescent nanolabels are needed.

Fluorescence nanolabels like organic fluorescence dyes and quantum dots (QDs) are widely used in single-molecule fluorescence detection. Usually, such as in immunodetection, fluorescence dye molecules are coupled to antibodies to generate a detectable signal, which possess the shortcomings of the low fluorescence signal intensity and the poor photostability [18]. The low fluorescence intensity results in a low signal-to-noise ratio which makes it difficult to identify the targets. In addition, most organic dyes suffer from serious self-quenching and photobleaching, which can lead to weak fluorescence intensity and weaker detection. High shortcomings limit the sensitivity of single-molecule fluorescence detection. To solve these problems, QDs have been employed as fluorescence nanolabels in single-molecule detection [19,20]. QDs are semiconductors that possess unique photophysical properties, such as high fluorescence intensity, continuous excitation spectra, narrow and tunable emission, and high photostability [21]. Although QDs have these unique prominent properties [22,23], there are still several problems such as blinking, physical adsorption, the stability of multifunctionalized QDs in different reaction systems and the toxicity of heavy

* Corresponding author. Tel.: +86 531 88362588; fax: +86 531 88564464.
E-mail address: wjiang@sdu.edu.cn (W. Jiang).

http://dx.doi.org/10.1016/j.talanta.2014.03.032
0039-9140/

metal ions [8,12]. Thus, to develop a new fluorescence nanolabel with high fluorescence intensity and excellent photostability which can avoid the shortcomings of QDs is highly desirable.

DNA nanostructure based fluorescence nanolabel was assembled by inserting fluorescence dyes into DNA nanostructure [24]. Benvin et al. have assembled linear and branched DNA nanostructure by DNA strands to serve as a template to accumulate the dyes [25]. Organic fluorescent dyes were embedded within these templates to assemble fluorescence nanotags [14,26]. The accumulation of dyes not only increases the fluorescence intensity but also prevents self-quenching [25]. Because the conjugation of DNA strands and dyes can form a rigid plane with electron cloud, the fluorescence intensity increases significantly. Due to high densities dyes can intercalate up to every other base pair, avoiding self-quenching by confining the dyes within separate intercalation sites [25]. However, these linear or branched DNA nanotags still undergo photobleaching. Compared with linear or branched DNA nanotags, DNA tetrahedron-based nanotag was more photostable, which may be due to the less efficient singlet oxygen production and low inherent reactivity toward singlet oxygen [27]. Furthermore, compared with QDs, DNA tetrahedron-based nanotags show good biocompatiblity and exhibit no blinking. As far as we know, despite the excellent properties of DNA tetrahedron-based nanotag, it has not been used in the detection of biomolecules. We employed it for the first time in the single-molecule detection.

In this work, we present a sensitive fluorescence immunoassay method for the quantitative detection of single protein molecules by employing DNA tetrahedron nanolabels to generate a detectable signal. The use of DNA tetrahedron nanolabels in SMD can avoid the shortcoming of QDs and overcome the limitations of organic dyes by preventing self-quenching and increasing the fluorescence intensity and photostability. The principle of this method is shown in Scheme 1. In this method, bio-nanolabels were attached to the streptavidin-rabbit antihuman antibody through the high-specificity, high-affinity biotin–streptavidin interaction. Human IgG captured on the epoxy-terminal was detected by its immunoreaction with the streptavidin-antihuman antibody. EFM with electron multiplying chargecoupled device (EMCCD) camera was employed for fluorescence imaging. Finally, the number of fluorescent spots on the image corresponding to the single target molecules was counted. The linear relationship between the total number of the spots and the concentration of the target was 3.0×10^{-14} to 1.0×10^{-12} mol L^{-1}.

2. Experimental

2.1. Reagents and materials

Human immunoglobulin G (IgG) and streptavidin-rabbit antihuman antibody (SA-Ab) (Number: RSb-0296P) were purchased from Abcam (HK) Ltd. (HK, China). DNA-intercalating dye SYBR Green I was purchased from Bio Teke Co. (Beijing, China). Tris (> 99.8%) was purchased from Amresco Inc. (Solon, OH). Tween-20, Bovine serum albumin (BSA) and 3-glycidyloxypropyltrimethoxysilane (GOPS) were purchased from Sigma-Aldrich Co. (St. Louis, MO, USA). Microscope cover glasses (22 mm × 22 mm) were purchased from Cole-Parmer (Illinois, USA). DNA oligonucleotides were purchased from Sangon Biotech Co., Ltd. (Shanghai, China). The sequences used for assembling the tetrahedron nanostructure are shown below: strand A: 5′-ACA TTC CTA AGT CTG AAA CAT TAC AGC TTG CTA CAC GAG AAG AGC CGC CAT AGT A-3′; strand B: 5′-TAT CAC CAG GCA GTT GAC AGT GTA GCA AGC TGT AAT AGA TGC GAG GGT CCA ATA C-3′; strand C: 5′-TTC AGA CTT AGG AAT GTG CTT CCC ACG TAG TGT CGT TTG TAT TGG ACC CTC GCA T-3′; and bio-strand D: 5′-Bio-TCA ACT GCC TGG TGA TAA AAC GAC ACT ACG TGG GAA TCT ACT ATG GCG GCT CTT C-3′. Other chemicals (analytical grade) were obtained from standard reagent suppliers.

The physiological buffer saline (PBS) consisted of 0.15 mol L^{-1} NaCl, 2.4×10^{-3} mol L^{-1} NaH_2PO_4, and 7.6×10^{-3} mol L^{-1} Na_2HPO_4 (pH 7.4). PBST buffer consisted of PBS and 0.05% Tween-20 (pH 7.4). TE buffer consisted of 1.0×10^{-2} mol L^{-1} Tris HCl and 1.0×10^{-3} mol L^{-1} Na_2EDTA (pH 8.0). TM buffer consisted of 2.0×10^{-2} mol L^{-1} Tris and 5.0×10^{-2} mol L^{-1} $MgCl_2$ (pH 8.0). TAE–Mg buffer consisted of 4×10^{-2} mol L^{-1}Tris, 2×10^{-2} mol L^{-1} Acetic Acid, 2×10^{-3} mol L^{-1} $EDTANa_2$ $12\ H_2O$, and 1.25×10^{-2} mol L^{-1} $(CH_3COO)_2Mg\cdot4H_2O$. A phosphate buffer (pH 7.4) containing 5% BSA was used as blocking buffer.

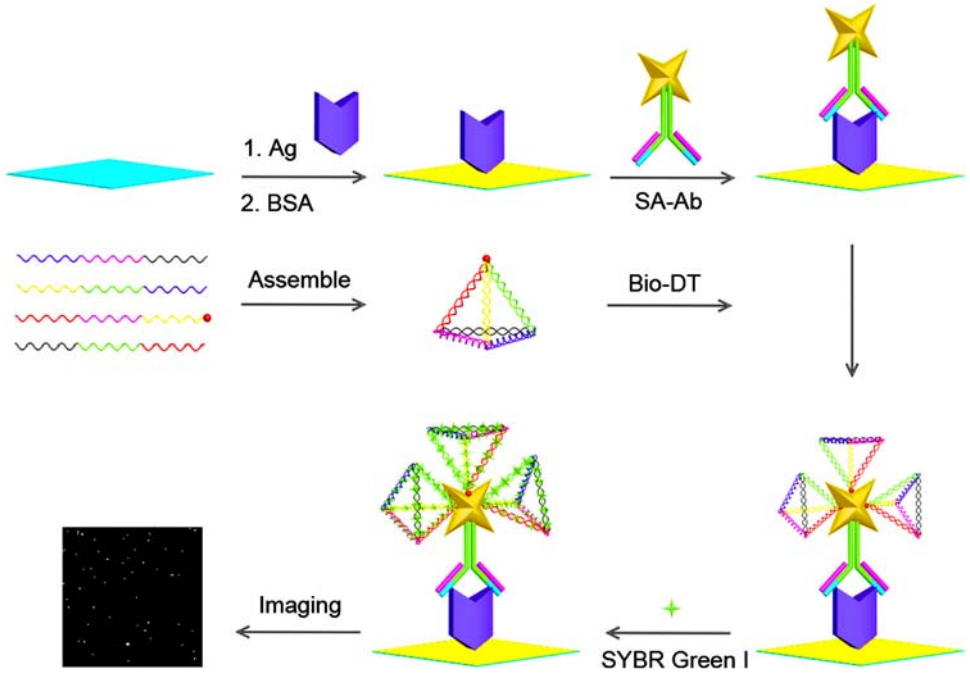

Scheme 1. The self-assemble of bio-DNA tetrahedron (Bio-DT) and the process of the detection of human IgG with DNA tetrahedron nanolabels. Ag represents antigen (human IgG), BSA represents Bovine serum albumin and SA-Ab represents the streptavidin-antihuman IgG antibody.

2.2. Apparatus

EFM imaging was performed with an Olympus IX81 fluorescence microscope (Tokyo, Japan) equipped with a high numerical aperture 60 × (1.45 NA) oil-immersion objective lens, a mercury lamp source, a mirror unit consisting of a 470–490 nm excitation filter (BP470-490), a 505 nm dichromatic mirror (DM 505), a 510–550 nm emission filter (IF 580), and a 16-bit thermoelectrically cooled EMCCD (Cascade 512 B, Tucson, AZ, USA). Imaging acquisition was performed using the MetaMorph software (Universal Imaging, Downingtown, PA, USA). All captured images were then further processed with an Analyze Particles function in a public-domain image-processing software ImageJ to determine the number of single fluorescence particlescount.

2.3. Self-assembly of DNA tetrahedron

Four DNA strands (A, B, C and bio-D) were diluted to a final concentration of 5.0×10^{-5} mol L^{-1} with TE buffer. A quantity of 2 μL of each strand was mixed with 42 μL of TM buffer; then the mixture was heated to 95 °C for 2 min, and rapidly cooled in ice bath.

2.4. Electrophoretic analysis of DNA tetrahedron

To verify the assembly of DNA tetrahedron, a polyacrylamide gel electrophoresis (native-PAGE) experiment was performed. Tetrahedrons were run on 12% native-PAGE gel in TAE–Mg buffer with a constant current of 35 mA at 4 °C.

2.5. Silanization of substrate surface and antigen immobilization

The epoxy-functionalized glass surfaces were prepared according to the modification described in the literature [8]. The freshly prepared substrate surface was coated with 100 μL human IgG solutions of various concentrations (1.0×10^{-12}, 5.0×10^{-13}, 2.0×10^{-13}, 1.0×10^{-13}, 5.0×10^{-14}, and 3.0×10^{-14} mol L^{-1}). The substrate was immediately placed in a sealed Petri dish at 37 °C for 12 h. After that, the substrate was washed three times with PBST and PBS washing buffers to remove unbound human IgG and impurities.

2.6. Blocking

A phosphate buffer containing 5% (W/V) BSA was used as the blocking buffer. The blocking buffer (100 μL) was added to the antigen coated substrate, and then, the substrate was incubated at 37 °C overnight. After that, the substrate was washed three times with PBST and PBS washing buffers.

2.7. Immunoreaction

In this work, 100 μL solution with different concentrations of SA-Ab (3.0×10^{-11}, 1.5×10^{-11}, 6.0×10^{-12}, 3.0×10^{-12}, 1.5×10^{-12}, and 9.0×10^{-13} mol L^{-1}) was added to the substrate. After that, the substrate was deposited hermetically for 2 h at 37 °C. Finally, nonspecifically absorbed antibodies were washed with PBST and PBS washing buffers.

2.8. Binding of bio-DNA tetrahedron to SA-Ab

The self-assembled DNA tetrahedron was diluted to a proper concentration with the phosphate buffer (pH 7.4). Then, 100 μL of the diluted solution (2.0×10^{-11} mol L^{-1}) was added to the substrate. Then, the substrate was immediately placed in a sealed Petri dish at 37 °C for 2 h. Finally, unbound tetrahedrons were washed with PBST and PBS washing buffers.

2.9. Addition of SYBR Green I and fluorescence imaging

In this step, 100 μL of SYBR Green I (2.0×10^{-7} mol L^{-1}) was added to the substrate and incubated for 15 min at room temperature. Tetrahedron fluorescent nanolabels were assembled by inserting SYBR Green I into DNA tetrahedron nanostructure, which was attached to the SA-Ab. In this case, DNA tetrahedron nanolabels were bound to a target, which produced fluorescent spots in the images. All images were taken using the Olympus IX81 microscope (60 × objective) equipped with a 16-bit thermoelectrically cooled EMCCD and the mercury lamp. The fluorescence images were obtained by the excitation light within the wavelength 470–490 nm. The exposure time was 100 ms, and the gain value was set at 2000. Finally, the bright spots corresponding to single protein molecules on the images were counted.

3. Results and discussion

3.1. Selection of fluorescent dye

In our work, DNA tetrahedron served as the template for the assembly of multiple intercalating dyes in a small well-defined region. For this strategy to work, the fluorescent dye must bind to DNA specifically. The binding stoichiometry should be high enough to ensure a high labelling ratio. What is more, the fluorescent dye should have suitable quantum yield. The quantum yield of the tetrahedron-bound probe should be comparable to that of the commonly used fluorescent dyes, such as rhodamine, Cy-3, and Cy-5, which is in the range of 0.1 to 0.9. Finally, fluorescent dye that remains unbound to tetrahedron should be minimal so that the immunoassay can be quantified in a low background without washing.

SYBR Green I was selected as the fluorescent probe in our work. It is a kind of intercalating dye that can only bind to double-strand DNA at a ratio of 1:2 [28]. The quantum yield dramatically increases when it binds to double-strand DNA. Cosa et al. have revealed that SYBR Green I had the quantum yield of 0.69 when bound to double-stranded DNA and the fluorescence intensity increased over 1000-folds [29]. As shown in Fig. 1, the fluorescence intensity of DNA tetrahedron nanolabels had a substantial increase compared to that of the free SYBR Green I. The maximum

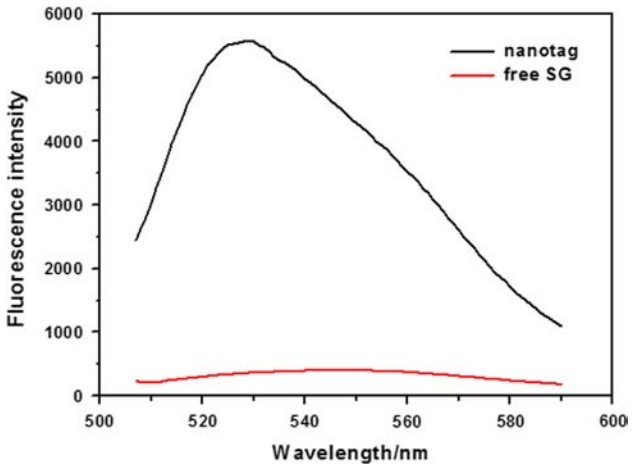

Fig. 1. Fluorescence spectra of free SYBR Green I (SG) and DNA tetrahedron nanolabels. The maximum absorption wavelength of DNA tetrahedron nanolabels is at about 525 nm.

excitation wavelength of DNA tetrahedron nanolabels was about 525 nm.

3.2. Self-assembly and characterization of DNA tetrahedron nanolabels

Tetrahedron nanolabels were assembled by the incubation of SYBR Green I and DNA tetrahedron. The self-assembly of DNA tetrahedron was first reported originally by Goodman et al. via a high-yield, single-step synthesis [30,31]. Four oligonucleotide strands of 55 bases each with partially complementary sequences were assembled into a tetrahedron. The tetrahedron consists of six edges of 17 base pairs which are connected by two unpaired nucleotides to ensure sufficient flexibility. Due to steric constraints, DNA helix must be stretched and unwound to create an intercalation site [27]. Intercalation dye saturates as one intercalator for every two base pairs. Thus, every edge can bind 8 intercalator dyes, and the whole 102 bases pairs in the tetrahedron can accommodate up to 48 intercalator dyes.

The assembling of DNA tetrahedron was verified by the native-PAGE (Fig. 2). DNA tetrahedron migrated more slowly than the single strand DNA and any other combinations lacking one or two strands, which corresponds to previous reports [32,33]. This confirmed the successful assembling of tetrahedron nanostructure.

After the assembling of DNA tetrahedron, the nanolabel was formed by the incubation of DNA tetrahedron and SYBR Green I for 15 min at room temperature. The dye molecules can bind to the double strand of DNA tetrahedron to increase the fluorescence intensity and photostability. After incubation, EFM was employed to observe the nanolabels. As shown in Fig. 3, each bright spot represents a nanolabel that exhibits no blinking.

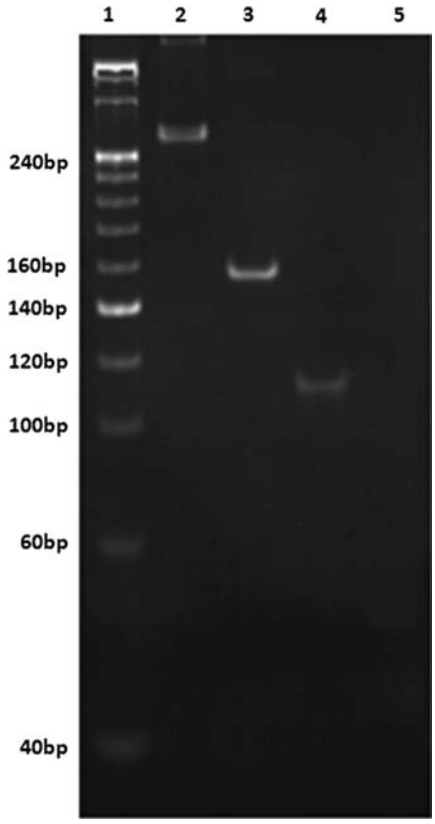

Fig. 2. Characterization of DNA tetrahedron on polyacrylamide gel electrophoretic (PAGE). Line 1: marker; line 2: A+B+C+D; line 3: A+B+D; line 4: A+B; and line 5: A.

Fig. 3. EFM fluorescence image of DNA tetrahedron nanolabels on the substrate. Scale bar 10 μm.

3.3. Nonspecific adsorption and blocking

In SMD experiments, at the end of every step, the unbound substance was washed with PBST and PBS. However, there were still a few molecules bound to the surface, which caused the nonspecific adsorption. The main substance that caused the nonspecific adsorption was the intermediate and fluorescent labels (QDs). Nonspecific adsorption generates false positive identification, which has an opposite effect on the sensitivity and accuracy of the assays. Therefore, it is crucial to decrease the false positive signal for the development of single-molecule immunoassays. The common method is using blocking agents to reduce the nonspecific adsorption.

Here, the nanolabels had no nonspecific adsorption on the substrate surfaces. Thus the main substance that caused nonspecific adsorption was SA-Ab. A commonly used blocking agent, BSA, was employed to reduce the nonspecific binding. After the antigen was bound on the epoxy group derivatived surface, BSA was added to block the unbound active site. Negative-control experiments were carried out at every concentration. To obtain the optimal blocking time, BSA was incubated for 4 h, 6 h, 8 h, 10 h and 12 h. Then the SA-Ab and fluorescent nanolabels were added successively before imaging analysis. The counted average bright spots of 10 images of negative-control experiments are shown in Fig. 4. Before 6 h of incubation, the negative signal had a sharp decrease, and approached a constant value after 8 h in two different concentrations of human IgG. At last, 12 h was selected as the optimum time for the incubation of BSA.

3.4. Single-molecule imaging analysis

EFM as an inexpensive light source of mercury lamp was empolyed here, which provides a convenient and alternative method for quantitative SMD analysis. To obtain an excellent resolution of single fluorescent spots in the fluorescence images, the study was optimized at a variety of imaging conditions. First, the exposure time and intensifier gain value were optimized to 100 ms and 2000, respectively. In this case, the optimal fluorescence image was obtained.

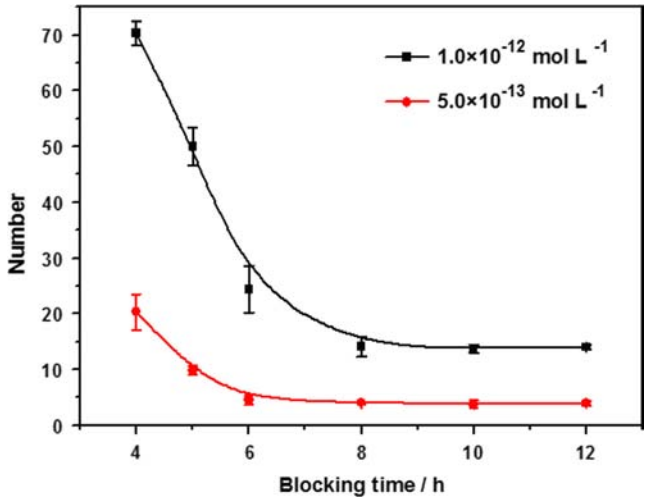

Fig. 4. Number of fluorescence spots responding to the blocking time of BSA at two different concentrations of human IgG. The line with square spots represents the concentration of 1.0×10^{-12} mol L^{-1}; The line with circular spots represents 5.0×10^{-13} mol L^{-1}. (For interpretation of the references to color in this figure legend, the reader is referred to the web version of this article.)

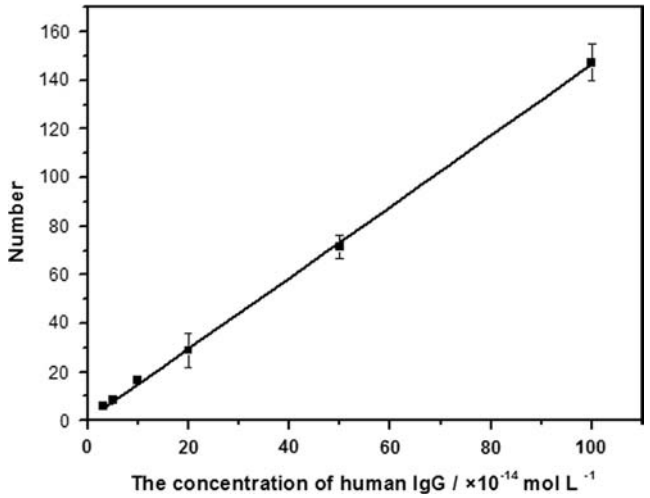

Fig. 5. Relationship between the number of single-molecules and the concentration of human IgG. The concentration of IgG is from 3.0×10^{-14} mol L^{-1} to 1.0×10^{-12} mol L^{-1}. Each data point represents an average of three measurements (each error bar indicates the standard deviation); 10 images for each measurement.

Second, in the experiment, the fluorescence intensity must be uniform to overcome the limitations of the nonuniform illumination region by mercury lamp through the objective. EMCCD has an imaging region of 512×512 pixels, and the light intensity disperses from the center. Therefore, a 150×150 pixels subregion at the center of the light was slected for measuring the fluorescence intensity image. With the 60× objective, each pixel imaged 0.33×0.33 μm^2 in the objective plane. The intensity deviation inside this subregion at the center of the light spot was less than 5%.

The images were obtained by the MetaMorph software. To ensure the accuracy and reproducibility of the results of single-molecule counting, the acquired subframe images needed a further handling with the Analyze Particles function in the ImageJ software to count the bright spots in every image. The threshold for image acquirement was chosen at a value of 3 times the standard deviation of the mean intensity for 10 blank images. For each concentration, 10 images were obtained from one location to the other on the substrate surface, which were acquired by moving the XY sample stage. The typical fluorescent subframe images of the blank substrate surface and target positive experiment corresponding to negative-control experiment at different concentrations in the range from 3.0×10^{-14} to 1.0×10^{-12} mol L^{-1} are shown in Fig. S1.

3.5. Quantification of antigen

To evaluate the detection performance of DNA nanolabels, human IgG was selected as a model analyte in our experiment. Under optimal conditions, 10 subframe images of each concentration were obtained for postive and negtive-control experiments. After setting the optimal threshold, we defined target molecules as sets of pixels that have intensity values greater than those of the threshold and every pixel is contiguous with other pixels within that spot. Thus, one fluorescence spot was considered as a target molecule. The concentration of human IgG was quantified by counting the number of bright spots corresponding to single molecules on the fluorescent subframe images. The total number of bright spots in each image was counted one by one. The molecule number corresponding to human IgG concentration was acquired via the total number of molecules in positive experiments subtracted from that in negative-controls. As shown in Fig. S1 the number of fluorescence spots on the positive images increased with the concentration of target immobilized on the substrate. Fig. 5 shows the linear relationship between the human IgG concentration and the number of molecules in the range of 3.0×10^{-14} to 1.0×10^{-12} mol L^{-1}, the correlation coefficient is 0.9997. Precision of the method was evaluated by analyzing the sample solution at a concentration of 1.0×10^{-12} mol L^{-1} and the relative standard deviation (R.S.D.) was 5.09% ($n=3$).

It is noted that the pixel area of a few brighter spots is larger than the mean area of a single spot corresponding to a single molecule. This may be because the distance between two targets was small and the two nearest fluorescent spots aggregated to form one brighter spot due to the diffraction of the fluorescence image. The higher the concentration, the more the large spots. The number of larger spots corresponding to several antibody molecules increased at higher concentrations, which may result in an uncorrected single-molecule counting and a deviation from the linearity. Therefore, the concentration of 1.0×10^{-12} mol L^{-1} was determined as the upper limit of linearity in this experiment. Estimation of the detection limit depends on the number of subframe images that are used for counting. It should be ensured that the number of molecules in positive experiments was at least two times that of negtive ones. In negative-control images, as the concentration of target decreases, the number of fluorescence spots decreases to null. Thus, at the detection limit, there should be at least one spot in the postive images. Based on these conditions, the detection limit was decreased to 3.0×10^{-14} mol L^{-1}. This may be because of the immobilization of target molecules on the substrate surface, which offers a much increased probability to be detected when compared with the detection of molecules in free solutions. The latter often had a large diffusion rate and a short residence time in the detection volume.

The specificity and matrix effect were further examined. To evaluate the specificity of the assay for human IgG, an experiment was carried out in which the surface-immobilized protein was replaced with mouse IgG, rabbit IgG or BSA, while keeping the protein concentration the same as that for human IgG. The subsequent assay procedure was also the same as for human IgG. As illustrated in Fig. 6, at a protein concentration of 1.0×10^{-12} mol L^{-1}, 10 images were obtained from different locations on the substrate surface. The fluorescence spots on the images of mouse IgG, rabbit IgG and BSA sample were very low by

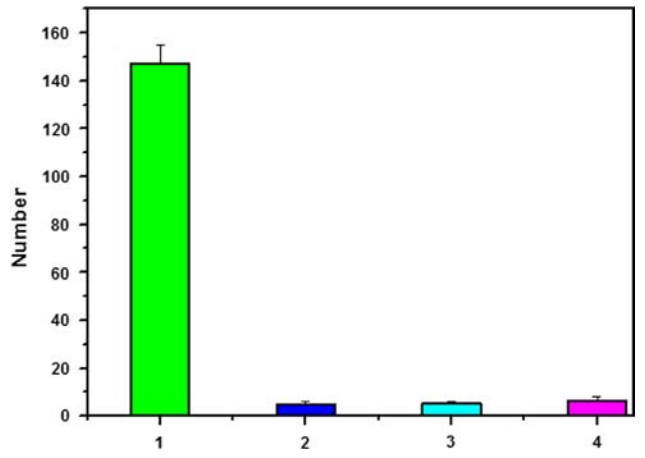

Fig. 6. Number of fluorescence spots corresponding to 1.0×10^{-12} mol L^{-1} human IgG (1), 1.0×10^{-12} mol L^{-1} mouse IgG (2), 1.0×10^{-12} mol L^{-1} rabbit IgG (3), and 1.0×10^{-12} mol L^{-1} BSA (4). Conditions: each data point represents an average of three measurements (each error bar indicates the standard deviation); 10 images for each measurement.

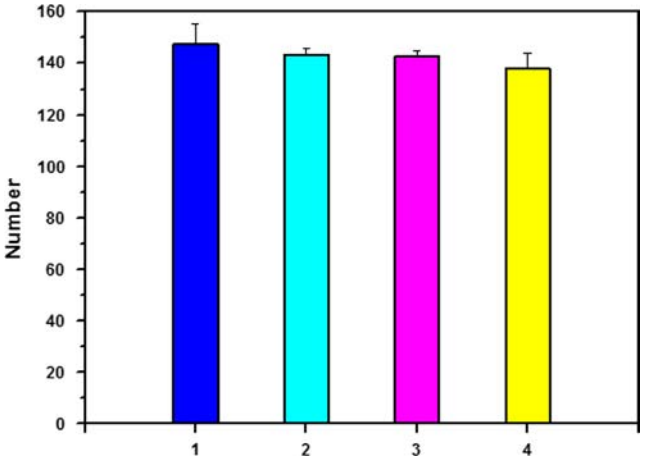

Fig. 7. Number of fluorescence spots corresponding to 1.0×10^{-12} mol L^{-1} human IgG in 1.46×10^{-1} mol L^{-1} Na^+ (1), 1.08×10^{-1} mol L^{-1} Cl^- (2), 5.3×10^{-3} mol L^{-1} K^+ (3), and 6.11×10^{-3} mol L^{-1} Glucose (4). Conditions: each data point represents an average of three measurements (each error bar indicates the standard deviation); 10 images for each measurement.

comparison with that of human IgG. The reason may be that the anti-human IgG antibody can only recognize human IgG peculiarly, which indicated that the immunoassay was highly specific for human IgG.

To examine the matrix effect, in this experiment, PBS buffer containing different components acted as the complex matrix. Several components in human blood were chosen as the complex matrix and the concentration of every component was chosen at the highest concentration in the blood. The PBS buffers containing 5.30×10^{-3} mol L^{-1} K^+, 1.08×10^{-1} mol L^{-1} Cl^-, 1.46×10^{-1} mol L^{-1} Na^+ or 6.11×10^{-3} mol L^{-1} glucose was used to dilute the human IgG. The concentration of human IgG and the subsequent assay procedure were the same as the former experiments. As illustrated in Fig. 7, the average number of bright spots of 10 images was obtained from different matrix effect experiments. The fluorescence spots did not show any significant difference indicating that there was very little interference of complex matrix on the designed strategy. The high specificity and low matrix effect could further ensure the practicality of the proposed strategy.

4. Conclusions

This article describes DNA tetrahedron/SYBR Green I as a new fluorescent nanolabel to detect human IgG by single-molecule counting. Tetrahedron fluorescent nanolabels were assembled by inserting SYBR Green I into DNA tetrahedron nanostructure which was self-assembled by four oligonucleotide strands. The fluorescence intensity of SYBR Green I increased thousand times when it bound to the DNA tetrahedron and the fluorescence became more photostable. The tetrahedron fluorescent nanolabel was employed to detect human IgG by fluorescence quantitative SMD. The images of the immobilized target molecules on the substrate surface were accomplished by an epi-fluorescence microscope and the MetaMorph software. The number of single fluorescent spots corresponding to single-molecules was counted in each image by the ImageJ software. The dynamic range of the number of fluorescence molecules corresponded to 2 orders of magnitude of target's concentration, and the detection limit of this single-molecule detection method was 3.0×10^{-14} mol L^{-1}. This method also has an excellent specificity and a low matrix effect. The bright photostable biocompatible DNA tetrahedron-intercalating dyes without blinking can be further used in bio-imaging.

Acknowledgment

We acknowledge the funding support from the National Natural Science Foundation of China (Grant nos. 21175081, 21175082, and 21375078).

Appendix A. Supporting information

Supplementary data associated with this article can be found in the online version at http://dx.doi.org/10.1016/j.talanta.2014.03.032.

References

[1] S.J. Weiss, L.V. Panlilio, J. Exp. Anal. Behav. 71 (1999) 13–24.
[2] X.X. Han, G.G. Huang, B. Zhao, Y. Ozaki, Anal. Chem. 81 (2009) 3329–3333.
[3] D.R. Walt, Anal. Chem. 85 (2013) 1258–1263.
[4] B. Sun, D.T. Chiu, Anal. Chem. 77 (2005) 2770–2776.
[5] J.P. Shelby, D.T. Chiu, Anal. Chem. 75 (2003) 1387–1392.
[6] Q. Huang, Z. Huang, G. Meng, Y. Fu, J.R. Lakowicz, Chem. Commun. (Camb.) (2013).
[7] Y. Fu, J. Zhang, J.R. Lakowicz, Chem. Commun. (Camb.) 48 (2012) 9726–9728.
[8] D. Jiang, L. Wang, W. Jiang, Anal. Chim. Acta 634 (2009) 83–88.
[9] L. Wang, G. Xu, Z. Shi, W. Jiang, W. Jin, Anal. Chim. Acta 590 (2007) 104–109.
[10] A.B. Loveland, S. Habuchi, J.C. Walter, A.M. van Oijen, Nat. Methods 9 (2012) 987–992.
[11] S. Lee, Y.H. Ko, H. Jung, J.D. Kim, J.M. Song, J. Choo, S.K. Eo, S.H. Kang, Talanta 78 (2009) 608–612.
[12] D. Jiang, C. Liu, L. Wang, W. Jiang, Anal. Chim. Acta 662 (2010) 170–176.
[13] D. Jiang, Q. Zhang, X. Shen, L. Wang, W. Jiang, Talanta 82 (2010) 1003–1009.
[14] Q. Xue, D. Jiang, L. Wang, W. Jiang, Bioconjug. Chem. 21 (2010) 1987–1993.
[15] Y. Fu, J.R. Lakowicz, Anal. Chem. 78 (2006) 6238–6245.
[16] X. Zhang, L. Li, J. Chen, G. Zou, Z. Si, W. Jin, Anal. Chem. 81 (2009) 1826–1832.
[17] L. Li, X. Tian, G. Zou, Z. Shi, X. Zhang, W. Jin, Anal. Chem. 80 (2008) 3999–4006.
[18] G. Yao, X. Fang, H. Yokota, T. Yanagida, W. Tan, Chemistry 9 (2003) 5686–5692.
[19] M.A. Hahn, J.S. Tabb, T.D. Krauss, Anal. Chem. 77 (2005) 4861–4869.
[20] C.Y. Zhang, L.W. Johnson, J. Am. Chem. Soc. 130 (2008) 3750–3751.
[21] J. Liu, Y. Liu, X. Yang, K. Wang, Q. Wang, H. Shi, L. Li, Anal. Chem. 85 (2013) 11121–11128.
[22] F. Zan, C. Dong, H. Liu, J. Ren, J. Phys. Chem. C 116 (2012) 3944–3950.
[23] H.T. Feng, W.S. Law, L.J. Yu, S.F. Li, J. Chromatogr. A 1156 (2007) 75–79.
[24] J. Li, C. Fan, H. Pei, J. Shi, Q. Huang, Adv. Mater. 25 (2013) 4386–4396.
[25] A.L. Benvin, Y. Creeger, G.W. Fisher, B. Ballou, A.S. Waggoner, B.A. Armitage, J. Am. Chem. Soc. 129 (2007) 2025–2034.
[26] Q. Zhang, L.H. Guo, Bioconjug. Chem. 18 (2007) 1668–1672.
[27] H. Ozhalici-Unal, B.A. Armitage, ACS Nano 3 (2009) 425–433.

[28] H. Zipper, H. Brunner, J. Bernhagen, F. Vitzthum, Nucleic Acids Res. 32 (2004) e103.
[29] G. Cosa, K.S. Focsaneanu, J.R. McLean, J.P. McNamee, J.C. Scaiano, Photochem. Photobiol. 73 (2001) 585–599.
[30] R.P. Goodman, R.M. Berry, A.J. Turberfield, Chem. Commun. (Camb.) (2004) 1372–1373.
[31] R.P. Goodman, I.A. Schaap, C.F. Tardin, C.M. Erben, R.M. Berry, C.F. Schmidt, A. J. Turberfield, Science 310 (2005) 1661–1665.
[32] H. Pei, N. Lu, Y. Wen, S. Song, Y. Liu, H. Yan, C. Fan, Adv. Mater. 22 (2010) 4754–4758.
[33] Z. Wang, Q. Xue, W. Tian, L. Wang, W. Jiang, Chem. Commun. (Camb.) 48 (2012) 9661–9663.